

Growth and characterization of ZnO nanostructured material

V. KHRANOVSKYY*, G. R. YAZDI, A. LARSON, S. HUSSAIN, P-O. HOLTZ, R. YAKIMOVA
 Linköping University, Department of Physics, Chemistry and Biology, 583 81 Linköping, Sweden

ZnO is a wide band gap (3.37 eV) semiconductor material with a high exciton binding energy (≈ 60 meV) at room temperature, which is a prerequisite for realization of efficient and stable optoelectronic systems. We demonstrated the APMOCVD growth of nanostructured ZnO material on Si and SiC with advanced emitting properties. The comparison of the properties of nanostructured polycrystalline layers with spatially disconnected ZnO nanocrystals clearly showed the advantage of the latter structures. Such structures distinctively luminesce in the UV range of the spectrum due to excitonic emission, while the contribution of the defect related luminescence is negligible. The significant improvement of the PL properties can be related to the decreased number of non-radiative recombination centers in the nanocrystals of high structural quality.

(Received September 1, 2008; accepted October 30, 2008)

Keywords: APMOCVD; Nanohexagons; Nanopillars; XRD, Photoluminescence.

1. Introduction

In recent years, much attention has been focused on zinc oxide (ZnO) as wide band gap semiconductor material because of its potential use in optoelectronics, transparent electronics (TCO), spintronics (DMS with high Tc) and nanotechnology [1]. Compared to GaN, ZnO is particularly attractive for UV-Blue light emitting devices (LED) due to the high exciton binding energy (≈ 60 meV) at room temperature, which is a prerequisite for realization of efficient and stable optoelectronic systems [2,3].

ZnO crystals of different forms and morphologies have been prepared by a number of techniques. Bulk ZnO crystals can be obtained via hydrothermal growth (HG) [4]. Thin ZnO films have been prepared by molecular beam epitaxy (MBE) [5], atomic layer deposition (ALD) [6], pulsed laser deposition (PLD) [7], chemical vapor deposition (CVD) [8] combined with metalorganic precursors (MOCVD) [9] or enhanced by plasma discharge (PECVD) [10], radio-frequency and direct current magnetron sputtering (RF and DC MS respectively) [11,12], etc. ZnO nanostructures have been fabricated by similar techniques via catalyst assisted vapor-liquid-solid (VLS) growth mechanism or direct vapor - solid mode [13-16]. Each technique has its advantages as well as disadvantages - therefore there is always a compromise between the technique simplicity and material quality, scalability and production costs, etc.

Since optical and electronic properties are highly sensitive to the crystalline quality of ZnO films, the choice of the substrate material has to be considered as well. Most of the substrate materials that are used today for ZnO growth (ScAlMgO₄ [17], SiC, Al₂O₃, ZnO) are, unfortunately, either too expensive or low scalable. Silicon substrates are cheap, technologically convenient and scalable, but the lattice and thermal expansion coefficient

mismatches are large for high quality ZnO growth [18, 19]. Thus, obtaining a high quality ZnO material on Si substrates is a challenging task. Furthermore, the development of simple and reliable Si integrated technique for deposition of device grade ZnO, matching optoelectronics requirements is of great importance.

There remain still some issues to be solved before the full commercialization of ZnO devices. First of all until now there are no reliable methods for p-type ZnO growth, although recently some groups have reported promising results [20-22]. Another difficulty is to obtain an efficient highly intensive luminescence from ZnO in the short wavelength range. Having a band gap of 3.37 eV, ZnO should emit in the range of 366 - 380 nm (A-UV radiation). Usually the emission spectra of ZnO consist of two luminescence bands: a narrow UV near band edge (NBE) excitonic emission and a broad deep level emission (DLE), so called "green" luminescence [23, 24]. The origin of DLE is still under debate but it is most probably related to Zn atoms as interstitials (Zn_i) and/or oxygen vacancies (V_o) [25]. Since for the application in optoelectronics a high emitting ability together with spectral purity of material is required, the above-mentioned problems should be solved. In a previous study [26] we have shown that in-situ hydrogen incorporation during growth of nanostructured ZnO films on Si results in suppression of DLE and an overall improvement of the emitting ability.

In the present paper we demonstrate an improvement of the luminescence properties for the case of nanosized ZnO crystals on Si and SiC. C-axis oriented nanopillars were grown on Si via self-assembled seeding layer while deposition on SiC resulted in epitaxially grown well defined hexagonal nanocrystals.

2. Experimental

2.1 Sample preparation

ZnO samples were prepared by atmospheric pressure metalorganic chemical vapor deposition (APMOCVD) in an experimental setup sketched in Fig. 1. Zn acetylacetonates ($\text{Zn}(\text{AA})_2$) and oxygen were used as precursors [27]. The setup consisted of a reaction chamber, subjected to a multi-zone heating (T_1 , T_2 , T_3), evaporator of Zn precursors and argon/oxygen inlets, equipped with gas flow meters. The substrate is located perpendicularly to the reagents flow in the T_3 temperature zone. Ar gas flow transports the vapor of thermally decomposed Zn precursor to the reaction zone, where due to mixing with oxygen, the ZnO deposits onto the substrate. The main technological parameters to be controlled are: substrate temperature ($T_s = T_3$), oxygen flow rate (Q_{O_2}), temperature of Zn precursor evaporation (T_{Zn}), argon flow rate (Q_{Ar}) and time of growth (t).

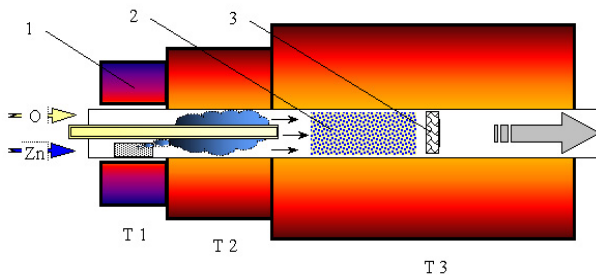


Fig. 1. Schematics of the APMOCVD setup for ZnO nanostructured material deposition. 1 – low temperature zone for Zn precursor evaporation; 2 – reaction zone; 3 – substrate;

A set of samples was prepared on Si (100) at substrate temperature ranging 350 – 500 °C. The estimated layer thickness was 200 – 250 nm. Also, a sample at a variable growth rate was prepared at $T_s = 500$ °C in a two-step procedure, allowing deposition of a continuous ZnO layer (seeding layer) followed by discontinuous nanostructures growth. Additionally, ZnO was grown on a p-type SiC substrate, which exhibits low mismatch and enables formation of p-n junction. All the samples prepared are listed in Table 1.

2.2 Characterization techniques

Scanning electron microscopy (SEM) was used to reveal the morphology and microstructure of the grown material (Leo 1550 Gemini SEM). The structural properties of the samples were measured by x-ray diffraction (XRD) using a Siemens D5000 diffractometer, utilizing $\text{Cu-K}\alpha$ radiation ($\lambda = 0.1542$ nm). From the perspective of future applications the microphotoluminescence measurements were carried out at room temperature with the frequency doubled Nd:YVO 4 laser as continuous wave excitation source, giving the wavelength $\lambda = 266$ nm. The laser was focused onto the sample with a reflecting microscope objective. The emitted luminescence was collected by the same objective and mirrored into a single grating 0.45 m monochromator equipped with a liquid nitrogen cooled Si-CCD camera with a spectral resolution of about 0.1 meV. The dimensions of the excited area was around 10 μm in diameter providing the excitation density 2 - 400 W/cm^2 .

Table 1. List of samples, prepared by APMOCVD and the main deposition parameters. NPs – nanopillars, HEX – hexagonal nanocrystals.

#	Sample	T_s , °C	Q_{O_2} (sccm)	T_{Zn} , °C	Q_{Ar} (sccm)	t , min
1	ZnO/Si/350	350	50	160	200	10
2	ZnO/Si/450	450	50	160	200	10
3	ZnO/Si/500	500	50	160	200	10
4	ZnO/Si/500 (NPs)	500	50	160-120	200	10
5	ZnO/SiC/500 (HEX)	500	50	120	200	10

3. Results and discussion

ZnO deposited on Si (samples 1-3) were found to be the layers of polycrystalline nature, consisting of nanosized grains. For sample 1, deposited at $T_s = 350$ °C, the grains are of smaller size – comparing to those deposited at 450 and 500 °C. Also, the uniformity of grain size is poor – the grains of different size are present. The samples, deposited at 450 and 500 °C display rather similar microstructure: the polycrystalline grains are well shaped and more uniform in size. However, still some

randomly distributed big grains are present (Fig. 2a-c). The two-step deposition on Si substrate resulted in growth of thin (about 100 nm) polycrystalline layer of ZnO, with a tiny elongated pillar on the top of each grain (Fig. 2d). The ZnO NPs are of similar diameter (≈ 35 nm) and length (≈ 150 nm) and are uniformly distributed over the surface. The obtained structures resulted from the two-step growth: at the first stage, at high reagents flow the polycrystalline seeding layer was formed. At the second stage, a small flow of reagents was introduced and at sufficient temperature it has a high migration ability to form the

structure of minimal surface energy. Thus, the ZnO nanopillars (ZnO NPs) growth was realized. The growth of ZnO on SiC substrate at lower reagents flow resulted in the growth of hexagonally shaped ZnO crystals (ZnO HEX) with lateral size ≈ 280 nm and height ≈ 200 nm

(Fig. 2e). The obtained structures were *epitaxially* grown and the c-axis of ZnO coincides with the c-axis of the SiC. The ZnO HEX tend to coalesce eventually forming a continuous layer (Fig. 2f)

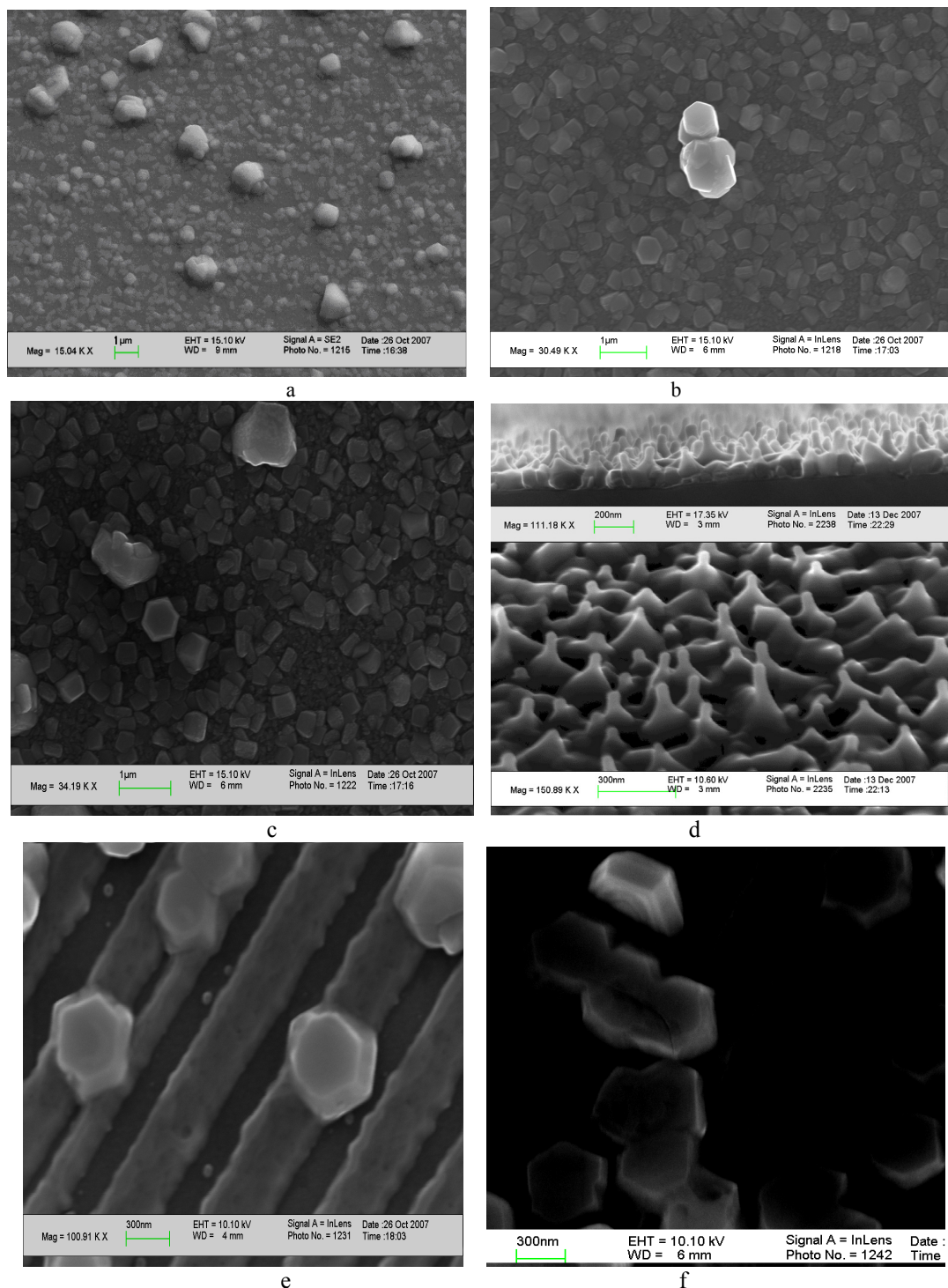


Fig. 2. SEM images (top view) of ZnO, deposited on Si substrates at a – 350, b - 450, c - 500 °C, d – ZnO nanopillars (top view and cross-section inset); e- ZnO HEX on SiC; f – ZnO HEX coalescence. The stripes represent steps on the SiC surface, which are decorated by ZnO deposit.

We have investigated the influence of deposition temperature on the crystal structure of ZnO/Si. The θ -2 θ

XRD spectra for the samples 1-3 are presented in Fig. 3a. The XRD data confirm the polycrystalline nature of the

films, showing the main reflections characteristic of ZnO wurtzite structure. With increase of the deposition temperature the XRD spectra become more developed: while for ZnO/Si deposited at 350 °C only the (002) peak of low intensity is present, for the sample deposited at 500 °C additional peaks appear – (100) and (101). This result is in agreement with the SEM observations.

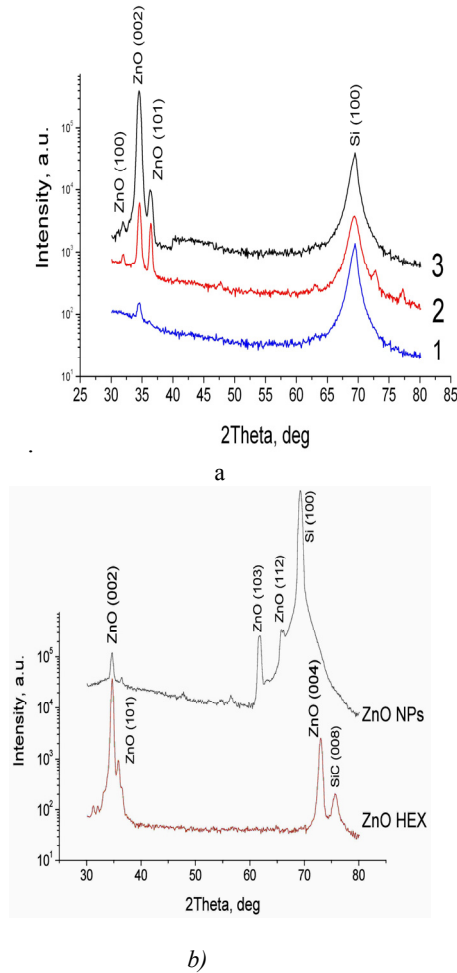


Fig. 3 a) The θ - 2θ XRD spectra of ZnO, deposited on Si substrates at 1 – 350, 2 - 450, 3 - 500 °C; b) The θ - 2θ XRD spectra of ZnO NPs and ZnO HEX.

Table 2. Data of XRD analysis for ZnO deposited on Si and SiC: peak position (2θ) of (002) reflection, interplanar spacing d , c -lattice constant, strain ε , stress G and (002) texture coefficient TC . All the data were calculated according to [30-37]. The standard value of c -lattice constant ZnO = 5.207 Å [38].

Sample/Substrate/Growth temperature (°C)	$2\theta_{(002)}$, deg.	d , Å	c , Å	ε , 10^{-3}	G , Gpa	TC
ZnO/Si/350	34.41	2.6049	5.2098	-0.59	+0.1420	1.01
ZnO/Si/450	34.49	2.5992	5.1984	-1.159	+0.3692	1.67
ZnO/Si/500	34.51	2.5975	5.1950	-2.24	+0.5195	2.09
ZnO/Si/500 (NPs)	34.55	2.5948	5.1896	-3.25	+0.7611	2.2
ZnO/SiC/500 (HEX)	34.60	2.5902	5.1805	-5.03	+1.1710	2.32

We explain the data obtained as following: at lower temperature of growth the surface mobility of atoms, adatoms and clusters is low and the species, reaching the substrate “freezing” and thus the obtained structure is polycrystalline with small grains. At increased temperatures (450-500 °C) the surface mobility of species to be deposited is higher and they are more able to find the most favorable place on the substrate surface, thus creating the well-shaped large crystallites that are textured to the substrate plane. The texture coefficient increases with increasing the deposition temperature (see Table 2.) The texture is formed due to self-textured growth – at the initial stage the grains with different orientations are formed, and then via competitive growth the grains, having the lowest surface free energy dominate [28]. Since the surface energy of (002) crystal plane is lowest calculated for ZnO [29], the grown films are textured with their c -axis perpendicular to the substrate plane

The XRD spectra of ZnO nanopillars (ZnO NPs) display peaks at (002), (103), (112) (Fig. 3b). We suggest, that the (002) reflection is mostly from the top part of the sample ZnO NPs, which are the elongated crystallites with their c -axis oriented perpendicular to the substrate. Probably, the (103) and (112) reflections come from the seeding layer. A unique feature of such structure is its fine size together with well ordering, uniformity and density. Moreover, the preparation of such structure without any catalyst is extremely prospective. The ZnO hexagons (ZnO HEX) are of high structural quality (see Fig. 3b): the commonly observed 002 peak has the second order reflection (004), what is characteristic of high quality crystalline materials and proves the single crystalline nature of ZnO HEX.

From the detailed analysis of the XRD data we have calculated the values of interplanar spacing c -lattice constant, strains and stress and texture coefficient for all the samples (Table 2).

It is evident that the c-lattice constant for all studied samples is less than the standard value for ZnO. We believe that this is due to the lattice and thermal expansion coefficient (TEC) mismatches. For ZnO in plane lattice constant $a = 3.252 \text{ \AA}$ and for cubic Si $a = 5.43 \text{ \AA}$. The TEC of ZnO is $6.51 \times 10^{-6}/\text{K}$ and for Si $\text{TEC} = 3.52 \times 10^{-6}/\text{K}$. Both factors influence and increase the value of the a-lattice constant, resulting in tensile strain. Since the a-constant increased, the c-constant decreased. This observation is also in agreement with the decrease of c-lattice constant with growth temperature increase. From Table 2 it follows that growth at higher temperatures causes larger strain and deformation of the ZnO grown on Si. Similar tendency is observed in the ZnO NPs sample, though with higher absolute values of the discussed parameters. Most probably, this is related to the dominant contribution from the seeding layer. The highest values of strain and stress were observed in the ZnO HEX. Because of the singly crystal nature of the hexagons and epitaxial relation with the substrate, they accumulate strain. While for polycrystalline structures the strains can partially release due to grain boundaries.

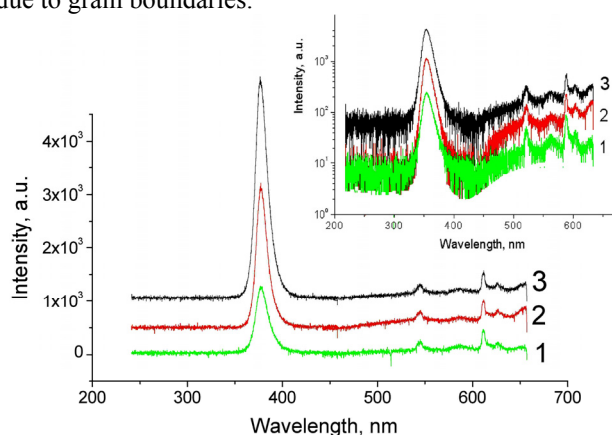


Fig. 4. RT PL spectra of ZnO/Si: 1- $T_s = 350 \text{ }^\circ\text{C}$; 2 - $T_s = 450 \text{ }^\circ\text{C}$; 3 - $T_s = 500 \text{ }^\circ\text{C}$. The sharp similar lines centered at 543 and 611 nm are due to background signal. Spectra are vertically shifted for better visualization. The inset represents the same spectra in log scale.

Besides the hexagonal shape of ZnO HEX, which reflects the ZnO crystal symmetry, we have obtained indications from the XRD measurements that the hexagons are epitaxially grown single crystals. Since the SiC substrates are 8° miscut from [0001], a signal from ZnO was obtained only after tilting the sample correspondingly. Also, we observed a possibility to assemble the single ZnO HEX's in two-dimensional layer (Fig. 2i). This feature is a good prerequisite for growth of single crystal ZnO films on SiC by boundary-free coalescence of well-oriented hexagonal crystallites.

We investigated the room temperature photoluminescence (PL) properties of the samples prepared. The RT PL spectra of ZnO deposited on Si at different temperatures are presented in Fig. 4.

All the spectra contain a sharp peak of the near band edge emission due to band-to-band transitions with maximum at 376 nm. Due to the broad defect emission, in the range 480 – 700 nm, it is difficult to identify the reasons causing it. With increase of the growth temperature the emitting ability of ZnO improves: the intensity of NBE emission increases monotonously, what can be due to a decreased concentration of non-radiative recombination centers as expected at high growth temperatures [23]. At the same time, the DLE intensity changes slightly. Due to the fact that at the present case growth occurred at O-rich conditions, the probability of oxygen vacancy presence is rather small. However, the growth temperature increase intensifies the growth rate, what can cause more intrinsic defects to appear at higher growth temperatures. In order to evaluate the contributions of NBE and DL emissions, we introduce a “figure of merit”, defined as $S = I_{\lambda(\text{NBE})} / I_{\lambda(\text{DLE})}$, where $I_{\lambda(\text{NBE})}$ is the integral spectral intensity of the NBE emission peak and $I_{\lambda(\text{DLE})}$ is the integral spectral intensity of the DLE peak. For the samples without obvious visible luminescence, $I_{\lambda(\text{DLE})}$ was calculated as the area of the background signal in the range 450–620 nm. Based on the figure of merit data, we may estimate the attraction of the grown material for optoelectronics. The summarized data deduced from the PL spectra are presented in Table 3.

Table 3. The data of RT PL of ZnO on Si and SiC.

Sample/ Substrate/Growth temperature ($^\circ\text{C}$)	NBE			DLE			S, a.u.
	I_{int}	λ , nm	FWHM, nm	I_{int}	λ , nm	FWHM, nm	
ZnO/Si/350	124158	377.1	15.0	120557	611.8	71.7	1.02
ZnO/Si/450	301864	377.5	14.5	160261	656.3	115.8	1.88
ZnO/Si/500	516892	376.5	13.3	182814	610.9	91.5	2.82
ZnO/Si/500 (NPs)	1733984	376.8	11.2	76387	---	---	22.7
ZnO/SiC/500 (HEX)	228276	376.9	12.8	43071	---	---	5.3

The ZnO nanostructures demonstrated advanced optical properties - high figure of merit: $S = 22.7$ for ZnO NPs and 5.3 for ZnO HEX. However, together with the

strong and narrow NBE PL, the ZnO NPs possess some defect related luminescence (Fig. 5). We assume, that most of DLE signal comes from the polycrystalline seeding

layer, while the intense NBE emission comes from the high quality ZnO NPs. Unfortunately, due to the tiny dimensions and high density of ZnO NPs it was not possible to determine the contribution of the seeding layer and NPs solely. In order to estimate the uniformity of the PL signal a mapping of the ZnO surface with a spot size $10 \times 10 \mu\text{m}$ was performed. For ZnO NPs the PL character and intensity were similar and perfectly uniform PL signal was observed. For ZnO HEX the PL character was similar, but the NBE intensity varied locally on different places of the sample, depending on the ZnO HEX density. It confirms that the photoluminescence observed comes from the hexagonal zinc oxide crystals.

In order to investigate the nature of luminescence of ZnO NPs and ZnO HEX we plotted the intensity of the NBE emission versus the excitation power ($I_{\text{NBE}} = f(P_{\text{exc}})$). The excitation power was changed from 2 to 400 W/cm^2 and the incident energy was focused on an area about $100 \mu\text{m}^2$.

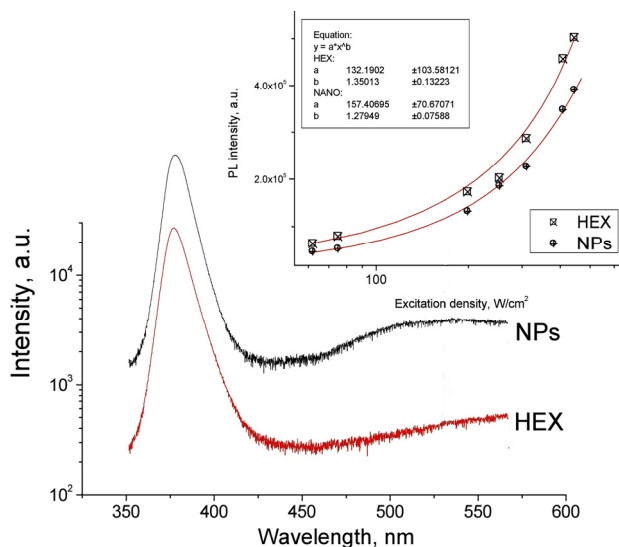


Fig. 5. RT PL spectra of ZnO NPs and ZnO HEX; inset is the excitation power dependence $I_{\text{NBE}} = f(P_{\text{exc}})$ for ZnO NPs and ZnO HEX.

By fitting the obtained experimental data by power function $I = P^k$, we extracted the power index k . For the ZnO NPs k value was found to be 1.27, while for HEX k equals 1.35. According to the model proposed by Schmidt [39] the observed luminescence is due to free and/or bound exciton emission. The photoluminescence data obtained demonstrate the potential of the prepared ZnO materials for such optoelectronic applications as light emitting devices and laser diodes.

4. Conclusions

ZnO polycrystalline layers consisting of nanosized crystallites can be grown by APMOCVD in a temperature

range $350 - 500 \text{ }^\circ\text{C}$ on bare Si substrates. All the as-grown nanostructured layers exhibit relatively low NBE emission and a broad “green-yellow” defect luminescence. Changing the morphology from nanostructured layers to spatially disconnected single nanocrystals (NPs, and HEX) leads to a significant improvement of the photoluminescence properties. The intensity of the NBE emission increases significantly, due to decreasing of the non-radiative recombination centers in the high structural quality nanocrystallites. The observed luminescence is of excitonic nature due to free and bound excitonic emission. We have elaborated a growth process for catalyst free fabrication of uniformly and densely distributed ZnO NPs on silicon substrates by using of ZnO seeding layer. Demonstrated epitaxial growth of ZnO single crystals on p-type SiC opens a possibility for processing of high-quality hetero p-n junction. The observed coalescence of ZnO HEX suggests a route toward ZnO epitaxial layer growth on foreign substrates.

Acknowledgements

The financial support from Swedish Institute and Swedish Research Council is greatly acknowledged.

References

- [1] Ü. Özgür, Ya. I. Alivov, C. Liu, A. Teke, M. A. Reshchikov, S. Doğan, V. Avrutin, S.-J. Cho, H. Morkoç, *J. Appl. Phys.* **98**, 041301 (2005).
- [2] S. Ishizuka, K. Suzuki, Y. Okamoto, M. Yanagita, T. Sakurai, K. Akimoto, N. Fujiwara, H. Kobayashi, K. Matsubara, S. Niki, *Phys. Status Solidi C* **1**, 1067 (2004).
- [3] Ya. I. Alivov, Ü. Özgür, S. Doğan, D. Johnstone, V. Avrutin, N. Onojima, C. Liu, J. Xie, Q. Fan, H. Morkoç, *Appl. Phys. Lett.* **86**, 241108 (2005).
- [4] K. Maeda, M. Sato, I. Niikura, T. Fukuda, *Semicond. Sci. Technol.* **20**, S49 (2005).
- [5] N. Izyumskaya, V. Avrutin, W. Schoch, A. El-Shaer, F. Reuss, Th. Gruber, A. Waag, *J. Cryst. Growth* **269**, 356 (2004).
- [6] C.-W. Lin, D.-J. Ke, Y.-C. Chao, L. Chang, M.-H. Liang, Y.-T. Ho, *J. Cryst. Growth* **298**, 472 (2007).
- [7] M. Okoshi, K. Higashikawa, M. Hanabusa, *Appl. Surf. Sc.* **154-155**, 424 (2000).
- [8] W.-C. Hou, B.-W. Lin, L. Chang, T.-S. Lin, C.-W. Lin, *phys. stat. sol. (c)* **1**, 856 (2004).
- [9] N. M. Sbrockey, S. Ganesan, *III-Vs Rev.* **17**, 23 (2004).
- [10] V. Khranovskyy, R. Minikayev, S. Trushkin, G. Lashkarev, V. Lazorenko, U. Grossner, W. Paszkowicz, A. Suchocki, B. G. Svensson, R. Yakimova, *J. Cryst. Growth* **308**, 93 (2007).
- [11] W. Wang, G. Diao, Z. Wang, M. Yang, T. Wang, Z. Wu, *Thin Solid Films*, **491**, 54 (2005).
- [12] W. Gao, Z. Li, *Ceramics Int.* **30**, 1155 (2004).

- [13] Z. L. Wang, *Mater. Today* **7**, 26 (2004).
- [14] Z. W. Pan, Z. R. Dai, Z. L. Wang, *Science* **291**, 1947 (2001).
- [15] X. Duan, Y. Huang, Y. Cui, J. Wang, C. M. Lieber, *Nature (London)* **409**, 66 (2001).
- [16] M. H. Huang et al. *Science* **292**, 1897 (2001).
- [17] T. Makino, C.H. Chia, N.T. Tuan, Y. Segawa, M. Kawasaki, A. Ohtomo, K. Tamura, H. Koinuma, *Appl. Phys. Lett.* **76**, 3549 (2000).
- [18] D.-Y. Lee, C.-H. Choi, S.-H. Kim, *J. Cryst. Growth* **268**, 184 (2004).
- [19] F. Xiu, Z. Yang, D. Zhao, J. Liu, K. A. Alim, A. Balandin, M. E. Itkis, R. C. Haddon, *J. Cryst. Growth* **286**, 61 (2006).
- [20] C. Wang, Z. Ji, J. Xi, J. Du, Z. Ye, *Materials Letters* **60**, 912 (2006).
- [21] E.-C. Lee, Y.-S. Kim, Y.-G. Jin, K. J. Chang, *Phys. Rev. B* **64**, 85120 (2001).
- [22] Look, D. C. & Claflin, B. *Phys. Status Solidi B* **241**, 624 (2004).
- [23] K. Vanheusden C. H. Seager, W. L. Warren, D. R. Tallant, J. A. Voigt, *Appl. Phys. Lett.* **68**, 403 (1996).
- [24] F. Leiter, H. Zhou, F. Henecker, A. Hofstaetter, D. M. Hoffman, B. K. Meyer, *Physica B* **308-310**, 908 (2001).
- [25] D.C. Look, J. W. Hemsky, J. R. Sizelove, *Phys. Rev. Lett.* **82**, 2552 (1999).
- [26] V. Khranovskyy, G. R. Yazdi, G. Lashkarev, A. Ulyashin and R. Yakimova, *Phys. Stat. Sol. A*, **205**, 1, 144 (2008).
- [27] V. Khranovskyy, U. Grossner, O. Nilsen, V. Lazorenko, G.V. Lashkarev, B.G. Svensson, R. Yakimova, *Thin Solid Films* **515**, 472 (2006).
- [28] V. Khranovskyy, U. Grossner, O. Nilsen, V. Lazorenko, G.V. Lashkarev, B.G. Svensson, R. Yakimova, *Thin Solid Films*, **515**, 472 (2006).
- [29] M. Ge, H. Wu, L. Niu, J. Liu, S. Chen, P. Shen, Y. Zeng, Y. Wang, G. Zhang, J. Jiang, *J. Cryst. Growth* **305**, 162 (2007).
- [30] B. Zhu, X. Sun, S. Guo, X. Zhao, J. Wu, R. Wu, J. Liu, *Jap. J. Appl. Phys.* **45**, 7860 (2006).
- [31] J. Hinze, K. Ellmera, *J. Appl. Phys.* **88**, 4567 (2000).
- [32] C. Wang, D. Xu, X. Xiao, Y. Zhang, D. Zhang, *J. Mater. Sc.* **42**, 123 (2007).
- [33] Y. G. Wang, S. P. Lau, H. W. Lee, S. F. Yu, B. K. Tay, *J. Appl. Phys.* **94**, 4329 (2003).
- [34] F. Akyuz, S. Kose, F. Atay, V. Bilgin, *Sem. Sci. Tech.* **21**, 1620 (2006).
- [35] H.-C. Hsu, C.-S. Cheng, C.-C. Chang, S. Yang, C.-S. Chang, W.-F. Hsieh, *Nanotechnology* **16**, 297 (2005).
- [36] S. Agouram, J. Bastos-Segura, V. Munoz-Sanjose, *Superlattices and Microstructures* **42**, 140 (2007).
- [37] S. Velumani, S. Narayandass, J. Mangalaraj, *Sem. Sci. Tech.* **13**, 1016 (1998).
- [38] Powder Diffraction File, JCPDS, ICDD, Newtown Square, PA, 2001, Card 36-1451.
- [39] T. Schmidt, K. Lishka, W. Zulehner, *PRB* **45**, 8989 (1992).

*Corresponding author: volkh@ifm.liu.se